JCSE The Journal of Corrosion Science and Engineering
ISSN 1466-8858 Volume 15, Preprint 31 submitted 4 July 2012

Effect of Chemical Composition on Uniform and Pitting Corrosion of Modified 9Cr-1Mo Ferritic Steels

M.G. Pujar*, T. Sakthivel#, U. Kamachi Mudali and K. Laha#
Corrosion Science and Technology Group
#Mechanical Metallurgy Division
Indira Gandhi Centre for Atomic Research
Kalpakkam – 603 102, India

∗ Corresponding author: pujar@igcar.gov.in

Phone: +91 44 27480121

Fax: +91 44 27480121

Abstract

Uniform corrosion, passive film dissolution and pitting corrosion resistance of different modified 9Cr-1Mo steels were studied as a function of chemical composition in general and Si content in particular. Uniform corrosion rates increased with increase in Si content in 0.5M H_2SO_4 solution; the increase in corrosion rates was delayed by increase in small amount of Cr. Passive film dissolution studies showed that there was no direct correlation of film dissolution time with Si content. However, it was observed that addition of Si had a direct influence on decreasing the pitting corrosion attack; thus, maximum pit radii decreased with increase in Si content of the steel.

Keywords: 9Cr-1Mo, chemical composition, silicon, chromium, pitting corrosion

Introduction

The chromium-molybdenum series of ferritic steels are used widely in the power generating, chemical processing, petroleum-processing industries because of their high strength at elevated temperatures combined with adequate toughness. Ferritic steel of 9 % Cr-1 % Mo is extensively used in the power generation industries due to its excellent mechanical properties and corrosion resistance. This steel, in the normalized and tempered condition has been favoured as a tubing material for fast reactor steam generators [1]. It has low thermal expansion and favourable mechanical properties at service temperatures and has a high resistance to stress corrosion cracking (SCC) in water-steam systems. In liquid-metal-cooled, fast breeder reactor applications, the carburization-decarburization possibility is low.

These considerations favoured the choice of 9 % Cr-1% Mo steel as the candidate material for tubing in the reheater and superheater portions and as a thick-section tube sheet material in the steam generator of a 500 MW(E) prototype fast-breeder reactor planned by Indian Atomic Energy Programme that is currently under construction at Kalpakkam. This material is being considered as the construction material for sodium-to-air decay heat exchangers to be used for emergency shutdowns. Because of the low cooling rate, low irradiation creep rate, and resistance to high-temperature embrittlement, material of this composition is also being considered for fast-reactor structural components, such as wrappers. The material undergoes degradation in properties as a result of long-term exposure to elevated temperature and aggressive environment. It is also susceptible to

JCSE The Journal of Corrosion Science and Engineering
ISSN 1466-8858 Volume 15, Preprint 31 submitted 4 July 2012

intergranular stress corrosion cracking (SCC) in environments where hydrogen is produced (e.g. general corrosion, welding and galvanic coupling with metals that are more active, such as carbon steel) [2-6]. Major as well as minor alloying elements have a strong influence on the uniform and localized corrosion properties of these steels. In the present investigation, six different modified 9Cr-1Mo ferritic steels were indigenously melted to study the effect of chemical composition on their corrosion properties. Although the effect of addition of many minor alloying elements has already been studied, effect of the addition of Si on 9Cr-1Mo is not studied earlier. Thus, in the present study steels with different Si contents from 0.17 to 0.44 wt.% were used. Although basic composition of the steels was similar, Cr content varied from 8.13 to 8.8 wt.%.

Experimental

The chemical composition of the steels is given in Table 1 and the steels are designated by their heat numbers. The chromium equivalent equation that uses the chemical composition (wt.%) of the alloy [7] is given below.

$$\begin{aligned} Net\ Chromium\ Equivalent = {} & (\%\ Cr) + \mathbf{6}\,(\%\ Si) + \mathbf{4}\,(\%\ Mo) + \mathbf{1.5}\,(\%\ W) + \mathbf{11}\,(\%\ V) + \\ & \mathbf{5}\,(\%\ Nb) + \mathbf{12}\,(\%\ Al\ soluble) + \mathbf{8}\,(\%\ Ti) - \mathbf{40}\,(\%\ C) - \mathbf{2}\,(\%\ Mn) - \mathbf{4}\,(\%\ Ni) - \mathbf{2}\,(\%\ Co) - \\ & \mathbf{30}\,(\%\ N) - (\%\ Cu) \end{aligned}$$

---------- (1)

Potentiodynamic anodic polarization studies

The calculated Net Chromium Equivalent values are also given in Table 1. The cylindrical specimens (10 mm diameter and 25 mm length) were used for all the investigations. The specimens were ground up to 1200 grit on the flat surface but polished up to fine diamond (1 µm) on the curved surface. Care was taken to round of the sharp edges in order to avoid the edge attack. The specimens were washed in soap solution and cleaned ultrasonically in methanol and dried before immersing in the solution. The time between the polishing and immersion in the solution was kept constant. The anodic polarization experiments were performed in five-necked polarization cell with a luggin-haber probe and a salt-bridge in order to establish the contact of the working electrode with the reference electrode. All solutions were prepared using double-distilled water. All the potentials were measured against saturated calomel electrode (SCE). Two platinum foils (with an area of 1 cm^2 each) spot-welded to the platinum wires were used as the counter electrode and were placed symmetrically on the opposite sides of the working electrode. The scan rate was chosen to be 0.1667 mV/s. The anodic polarization experiments were conducted in 0.5M H_2SO_4 solution open to atmosphere. Initially, the specimen was immersed in the solution for 45 min in order to observe the stable open circuit potential (OCP). Thereafter, the anodic polarization experiment was conducted starting from a cathodic potential of -0.75 V(SCE) till the specimen crossed the stage of secondary passivity.

Potential decay studies

In order to conduct the potential decay studies, the freshly polished specimen was first anodically polarized up to +500 mV(SCE) in 0.5M H_2SO_4 solution at a scan rate of 1 mV/s; thereafter the specimen was passivated at an applied potential of +500 mV(SCE) for 10 min which was followed by breaking the circuit to measure the potential decay till the potential

reached the OCP. The time to decay the potential to OCP which indicates the stability of the passive film was measured.

Electrochemical Noise (EN) studies

Electrochemical Noise (EN) studies were conducted in 0.05M sodium chloride solution open to atmosphere using two nominally similar specimens with same surface finish by galvanically coupling them using zero resistance ammeter (ZRA). The current noise was measured as a galvanic coupling current between the two electrodes. The potential noise of the coupled electrodes was measured against an external SCE. The EN signals were measured using Solartron 1287 equipment at 1 Hz sampling frequency for 24h continuously.

Extreme value statistical analysis

Extreme value analysis enables prediction of the most probable maximum extent of corrosion, for example, the deepest pit in the case of the pitting corrosion. Extreme value analysis is therefore well suited to localized corrosion because failure induced by localized corrosion usually occurs when any local site fails, that is when a single deepest pit perforates the wall of the structural material [8].
The 84 current EN data sets (each with 1024 data points) were used for extreme-value analysis. If the pits are assumed to be hemispherical the pit radii could be calculated using the following equations. The integration of current signal with time was used to determine the charge passed for each current transient. This charge is the result of the formation of a single metastable pit and can be related to the physical volume of the pit by using Faraday's equation given below,

$$Pit\ Volume = \frac{Q \times M_m}{F \times n \times D} \qquad 2)$$

$$Pit\ radius = \left(\sqrt[3]{\frac{3 \times V}{2\pi}} \right) \times 10{,}000 \qquad 3)$$

where, Q is the charge passed, M_m, is the molecular mass of the alloy, F is Faraday constant, n is the number of electrons released in each anodic reaction, D is the density of the alloy, V is the pit volume (cm^3) and pit radius is expressed in µm. If the pits are assumed to be hemispherical the pit radii could be calculated using equation 3 given above. The integrated charges associated with the largest current transient from each data set were used to calculate the pit radii. First, all the calculated extreme values of the pit radii were arranged in the descending order and then the cumulative probability F(Y) was calculated as 1- [M/(N+1)], where M is the rank of the ordered pit radii calculated using extreme values and N is the total number of the pit radii. The reduced variate (Y) can then be calculated by using formula Y = –ln{–ln[(Y)]} [9-15]. From the distribution parameters (µ and α) the values of the largest expected pit size (Pit_{max}) was calculated using the following equations (4),

T = A/a and $Pit_{max} = \mu + \alpha \ln T$ 4)

Where "A" is equal to the area over which a prediction is to be made and "a" is the area of the small specimens used in the laboratory to establish the distribution parameters; µ and α are the location and scale parameters for the distribution of the largest metastable pits respectively. The value of T was 1.01 in these calculations.

After the potentiodynamic polarization studies in 0.5M sulphuric acid medium the specimens were observed under optical microscope. Similarly, after EN studies, the specimens were electrochemically etched using 0.5M sulphuric acid at 1.5 V for 1s to know the pit morphology.

Results and Discussion

From the potentiodynamic anodic polarization curves (Fig.1), it is obvious that they appear similar irrespective of the chemical composition. The potentiodynamic anodic polarization curves have been marked with arrows, A-B, C-D and E-F indicating different regions. Region A-B shows the potential region of active dissolution and the one marked C-D shows the region of passivity, wherein a film of corrosion deposits protects the metal from undergoing corrosion. At point D, the steel start to undergo transpassive dissolution whereas the region E-F indicates the region of secondary passivity. The addition of Cr to pure iron leads to the decrease in the broad active peak spanning from -500 mV to 450 mV(SCE) to a single peak with 100% Cr; for the intermediate additions of Cr, the active peak shrinks slowly showing initially two peaks where decrease in the passivation potential, critical current density for passivation and passive current density are observed with increasing Cr content and the appearance of secondary passivity at about 1.0 V(SCE) due to the onset of the formation of CrO_4^{2-} [16]. The potentiodynamic anodic polarization diagram for a steel containing 10.5 wt.% Cr resembling Fig.1 is shown to be having two peaks [17] The critical anodic current density (I_{cc}) values were assessed and they did not show any trend with increase in the Si concentration but the values decreased as a function of Cr content as well as net Cr equivalent (Fig.2). A similar observation was made by Blajiev et al. [18] in their investigation on the Fe25Cr ferritic stainless steels containing 1-5 wt.% Si in 0.5M H_2SO_4, wherein the I_{cc} values did not show any variation. From the trend in Fig.2, it was obvious that minor variation in Cr had an overwhelming influence in decreasing the I_{cc} compared to other elements.

Uniform corrosion rates were determined using linear polarization technique (LPR) and the values were plotted as cumulative probability vs. corrosion rate plot (Fig.3). The steels with lowest Si contents like steels 4381 and 4382 with comparable Cr contents and having same Si contents (lowest) showed the lowest corrosion rate profiles. Steels 4385 and 4380 showed increased corrosion rates compared to steels 4381 and 4382 as they had higher Si contents of 0.38 and 0.24 wt.% respectively. Relatively lower corrosion rates of 4385 (even with relatively higher Si content of 0.38 wt.%) compared to 4380 can be explained based on the slightly higher Cr content in it than the latter. Steels 4384 and 4383 showed further increase in the corrosion rates which was attributed with 0.39 and 0.44 wt.% of Si respectively. Among these two steels 4384 showed lower corrosion rate due to the higher Cr content (8.8 wt.%) compared to 4383 (8.23 wt.%). Thus, it is apparent that Si increases the uniform corrosion rate of the steel, an observation supported by the earlier workers [18]. It was suggested by these authors that silicon absorbed a sufficient amount of electronic charge density from iron and chromium which led to increased strength of iron- and chromium-water adsorption complexes and facilitated their release into the solution.

Potential decay curves and potential decay times are shown in Fig.4 and Fig. 5 respectively. Since potential decay times did not show a trend with Si content of the steels, they were plotted as a function of Cr content as well as net Cr equivalent which takes into account the effect of all the elements. It was obvious that potential decay times increased with increase in Cr content linearly. The first five points in Fig.5 showing the potential decay against net Cr equivalent exhibit a moderate rise in the potential decay time indicating

somewhat adverse effect of Si on the passive film decay; the position of the fifth point is dictated more by the Cr content (which is highest and is 8.8 wt.%) rather than Si content. Thus, it appears that Si may not be as helpful as other major alloying elements (Cr, Mo) in stabilizing passive film.

These steels were in the normalized and tempered condition which consist of tempered martensitic microstructure. The photomicrograph taken after the potentiodynamic anodic polarization studies in 0.5M sulphuric acid (Fig.6) shows corrosion attack on the prior austenite grain boundaries. The photomicrographs of pitted specimens are shown in Fig. 7 and Fig. 8 for Steel-4381 and Steel-4382 respectively. Figure 7 shows extensive pits in Steel-4381 as compared to Steel-4382 which shows less number of pits. It was observed that the pits were preferentially initiated on the triple points of prior austenite grain boundaries. Parvathavarthini et al. [19] have shown that the martensite lath boundaries were predominant sites for the nucleation of pits.

The plots of the reduced variate (Y) versus the pit radii (μm) for different steels are shown in Fig.9. Steels M-4380 and M-4381 show single slope behaviour whereas other three steels show two-slope behaviour. The two slope behaviour of the pit radii versus the reduced variate (Y) plot has been explained by Zhang et al. [20, 21] as corresponding to the metastable (relatively smaller pit radii) and the stable pits (relatively larger pit radii) respectively. However, in the present investigation, the exact size of the metastable pits at which the transition from the metastable to stable pitting took place could not be decided. The μ and α values obtained from the single slopes are given in Table 2. From μ and α values given in Table 2 Pit_{max} values were calculated for different steels. Effect of Si content on the Pit_{max} is shown in Fig.10. It is quite clear that Si helps in decreasing the Pit_{max} values directly (the data for 4382 could not be obtained) signifying its direct role in inhibiting pitting corrosion in these steels. It is known that addition of Si as an alloying element improves the resistance of austenitic stainless steels to pitting corrosion [22-24]. Perez et al.[25] observed that above a critical dose, Si implantation on 304 resulted in delay in pit nucleation in 0.5M sodium chloride medium. The effect of Si implantation on pitting resistance is much more pronounced on 430 steel in the same medium.

Conclusions

From the above investigations the following conclusions were drawn.

1. Addition of Si increases the uniform corrosion rates. The potential decay studies showed that Si does not have a role in inhibiting passive film dissolution. Addition of Si did not show any influence in decreasing the I_{cc} values. However, Cr has an overwhelming effect on inhibiting the passive film dissolution.
2. Addition of Si had direct influence on inhibiting pitting corrosion of steels. Thus, Pit_{max} values were found to decrease linearly with increase in Si content of the steels.

References

1. R.L. Klueh, International Materials Reviews, Vol.50, No. 5, 2005, pp. 287-310.
2. C. A. Hippsley, N.P. Haworth, Materials Science and Technology, Vol. 4, No. 9, 1988, pp. pp. 791-802.
3. R. Kurahashi, T. Kurisu, Y. Sone , K. Wada, Y. Nakai, CORROSION/84, paper no. 212, NACE, Houston, TX (1984).
4. H. Kiesheyer, G. Lennartz, U.K. Natl. conf. 69, London, England, November 1982, Institute on Corrosion Science and Technology, Birmingham, U.K., 1982, p. 69.

ISSN 1466-8858 Volume 15, Preprint 31 submitted July 2012

5. S.K. Banerji, C.J. McMohan Jr., H.C. Feng, Metallurgical Transactions 9A, No.2, 1978, pp. 237-247.
6. S.K. Banerji, C.L. Briant, C.J. McMohan Jr., in Proc. Conf. Mechanisms Environment-Sensitive Cracking of Materials, (eds) P.R. Swann, F.P. Ford, A.R.C. Westwood, London, England: The Metal Society, 1977, p.437.
7. P. Patriarca, S.D. Harkness, J.M. Duke, L.R. Cooper, Nuclear Technology, Vol. 28, No. 3, 1976, pp. 516-536.
8. J. J. Vajo, R. Wei, A.C. Phelps, L. Reiner, G.A. Herrera, O. Cervantes, D. Gidanian, B. Bavarian and C.M. Kappes, Corrosion Science, Vol. 45, No. 3, 2003, pp. 497-509.
9. P. M. Aziz, Corrosion, Vol. 12, No. 10, 1956, p 495t.
10. T. Shibata, K. Okamoto, Boshoku Gijutsu, Vol. 34, No.7, 1981, pp. 404-408
11. T. Shibata, "1996 W.R. Whitney Award Lecture: Statistical and Stochastic Approaches to Localized Corrosion," Corrosion, Vol. 52, No. 11, 1996, pp. 813-830.
12. J.E. Strutt, J.R. Nicholis, B. Barbier, Corrosion Science, Vol. 25, No. 5, 1985, pp. 305-315.
13. G.P. Marsh, K.J. Taylor, Corrosion Science, Vol. 28, No.3, 1988, pp. 289-320.
14. Kowaka M (ed). Introduction to Life Prediction of Industrial Plant Materials: Application of the Extreme Value Statistical Method for Corrosion Analysis, Allerton Press, Inc., New York (1994).
15. A.R. Trueman, Corrosion Science, Vol. 47, No. 9, 2005, pp. 2240-2256.
16. R. Kirchheim, B. Heine, H. Fischmeister, S. Hofmann, H. Knote and U. Stoez, Corrosion Science, Vol. 29. No. 7, 1989, pp. 899-917.
17. D. Tao and B.K. Parekh, Florida Institute of Phosphate Research, Publication No.: 01-170-208, June 2004, FL, USA.
18. O. Blajiev, L. Chigirinskayab and G. Chernovab, Electrochimica Acta, Vol. 43, No, (1-2), 1998, pp. 199-202.
19. N. Parvathavarthini, R.K. Dayal, J.B. Gnanamoorthy, Corrosion, Vol. 52, No. 7, 1996, pp. 540-551.
20. Tao Zhang, Xiaolan Liu, Yawei Shao, Guozhe Meng and Fuhui Wang, Corrosion Science, Vol. 50, No. 12, 2008, pp. 3500-3507.
21. Tao Zhang, Chongmu Chen, Yawei Shao, Guozhe Meng, Fuhui Wang, Xiaogang Li and Chaofang Dong, Vol. 53, No. 27, 2008, pp. 7921-7931.
22. Tomashov N D, Chernova G P, Metallurgia, Moscow (1989).
23. J. Baszkiewicz, M. Kaminski, A. Podgrsky, J. Jagielki, G. Gaw- lik, Corrosion Science, Vol. 33, No. 5, 1992, pp. 815-818.
24. J. Baszkiewicz, J. A. Kozubowski, D. Krupa, Journal of Materials Science, Vol. 33, No. 18, 1998, pp. 4561-4568.
25. P´erez F J, Hierro M P, G´omez C, Mart´ınez L, Duday D, Surface and Coatings Technology, Vol. 133-134, 2000, pp. 344-350.

JCSE The Journal of Corrosion Science and Engineering
ISSN 1466-8858 Volume 15, Preprint 31 submitted 4 July 2012

Table 1: Chemical composition of the steels, wt.%

Element	Steel-4380	Steel-4381	Steel-4382	Steel-4383	Steel-4384	Steel-4385
Fe	89.669	89.551	89.66	89.272	88.775	89.281
Cr	8.13	8.35	8.2	8.23	8.8	8.33
Mo	0.95	0.95	0.96	0.95	0.93	0.94
V	0.21	0.22	0.22	0.22	0.23	0.22
Nb	0.08	0.07	0.07	0.08	0.08	0.08
C	0.095	0.093	0.092	0.09	0.092	0.094
N	0.026	0.026	0.028	0.039	0.033	0.026
Cu	0.01	0.01	0.01	0.01	0.01	0.01
Mn	0.37	0.35	0.37	0.45	0.45	0.44
S	0.004	0.004	0.004	0.003	0.004	0.003
P	0.005	0.005	0.005	0.005	0.005	0.005
Ni	0.21	0.2	0.21	0.21	0.2	0.19
Si	0.24	0.17	0.17	0.44	0.39	0.38
Al	0.001	0.001	0.001	0.001	0.001	0.001
Net Cr Eq.	**9.922**	**9.942**	**9.732**	**10.982**	**11.422**	**11.012**

Table 2: The values of μ and α obtained from the plots

Steel	μ	α
M-4380	10.65	5.01
M-4381	10.96	4.33
M-4383	8.63	3.29
M-4384	9.18	4.32
M-4385	9.13	4.59

JCSE The Journal of Corrosion Science and Engineering
ISSN 1466-8858 Volume 15, Preprint 31 submitted 4 July 2012

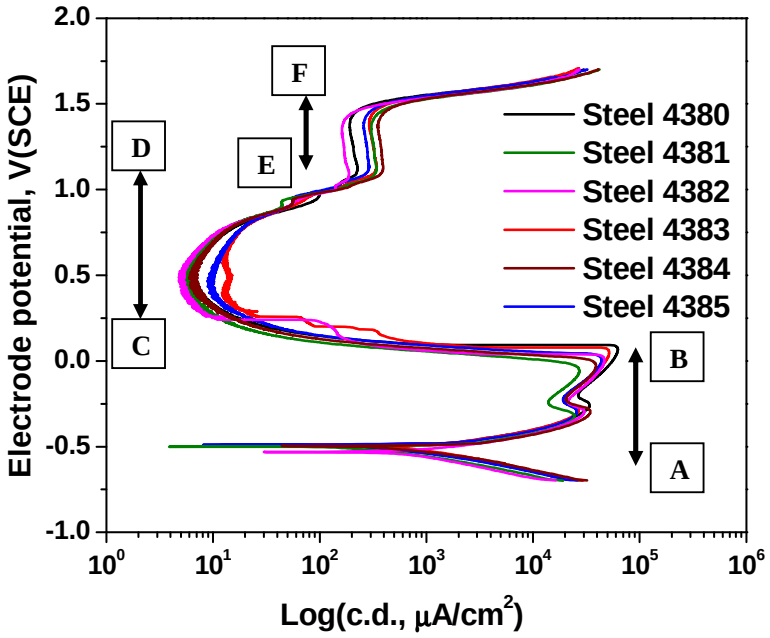

Fig.1	Potentiodynamic anodic polarization curves for the steels in 0.5M H_2SO_4

JCSE The Journal of Corrosion Science and Engineering
ISSN 1466-8858 Volume 15, Preprint 31 submitted 4 July 2012

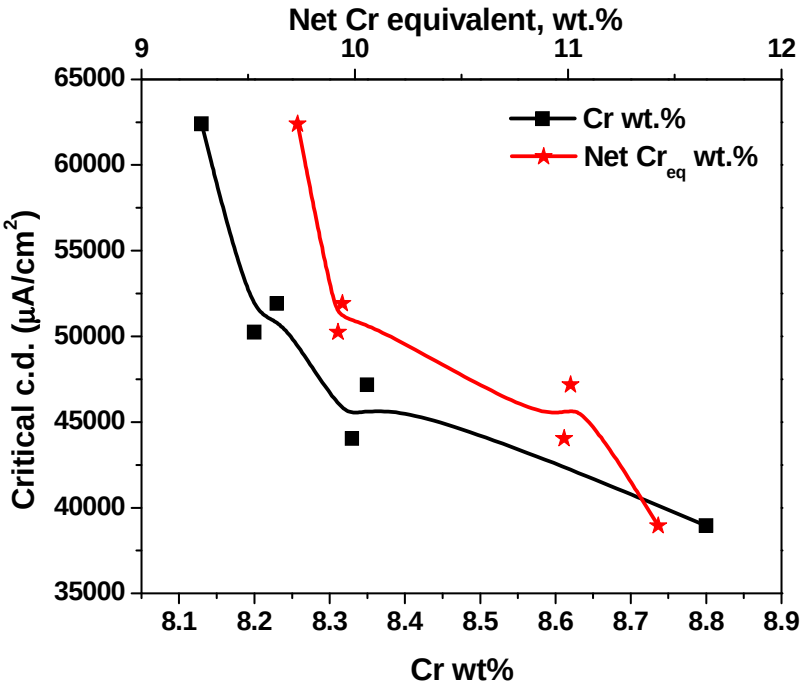

Fig.2	The plots of Icc as a function of both Cr and Net Cr equivalent for the steels in 0.5M H_2SO_4

JCSE The Journal of Corrosion Science and Engineering
ISSN 1466-8858 Volume 15, Preprint 31 submitted 4 July 2012

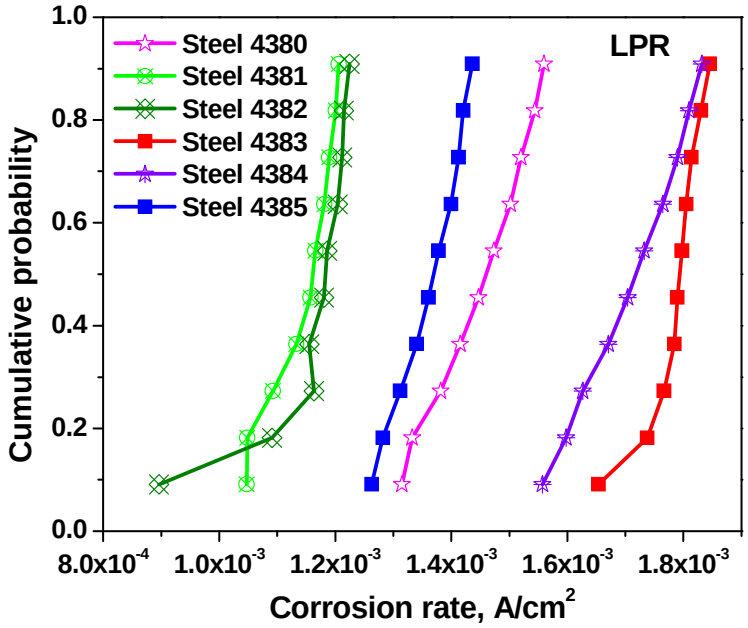

Fig.3	The plots of cumulative probability vs. corrosion rate for the steels in 0.5M H_2SO_4

JCSE The Journal of Corrosion Science and Engineering
ISSN 1466-8858 Volume 15, Preprint 31 submitted 4 July 2012

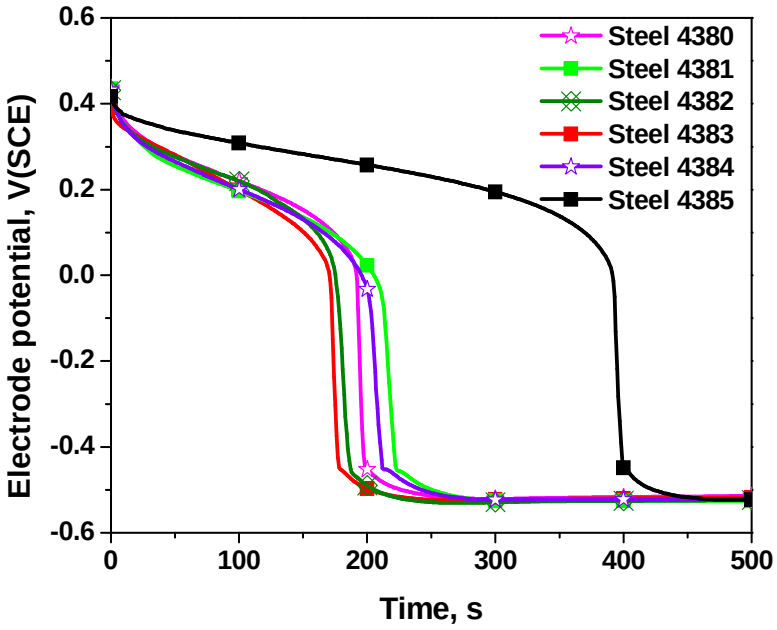

Fig.4	The potential decay curves for the steels in 0.5M H_2SO_4

JCSE The Journal of Corrosion Science and Engineering
ISSN 1466-8858 Volume 15, Preprint 31 submitted 4 July 2012

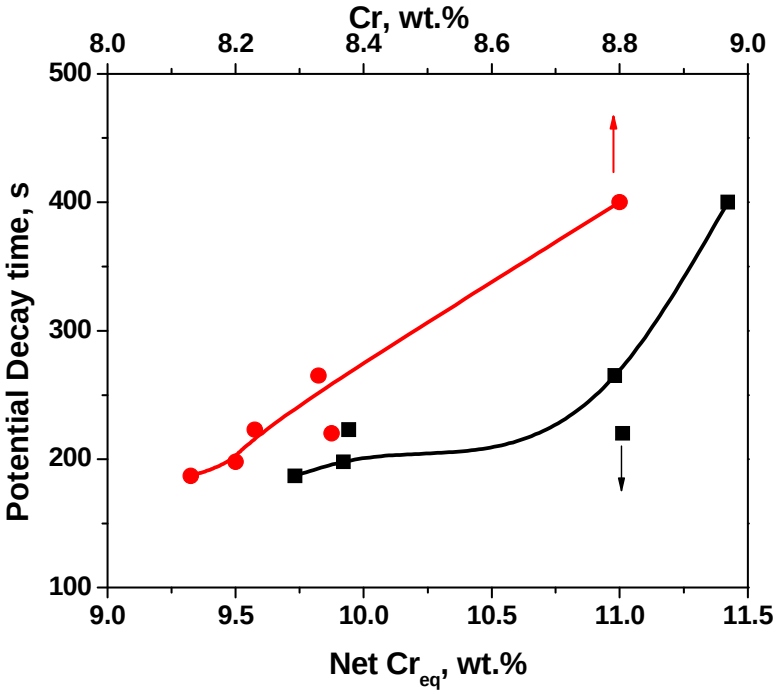

Fig.5	The potential decay time vs. Cr as well as net Cr equivalent for the steels in 0.5M H_2SO_4

JCSE The Journal of Corrosion Science and Engineering
ISSN 1466-8858 Volume 15, Preprint 31 submitted 4 July 2012

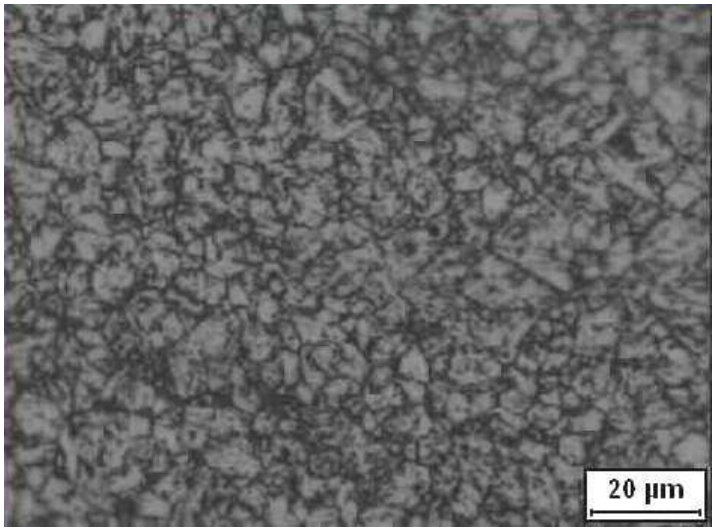

Fig.6	The photomicrograph of Steel-4383 after potentiodynamic anodic polarization experiment in 0.5M H_2SO_4

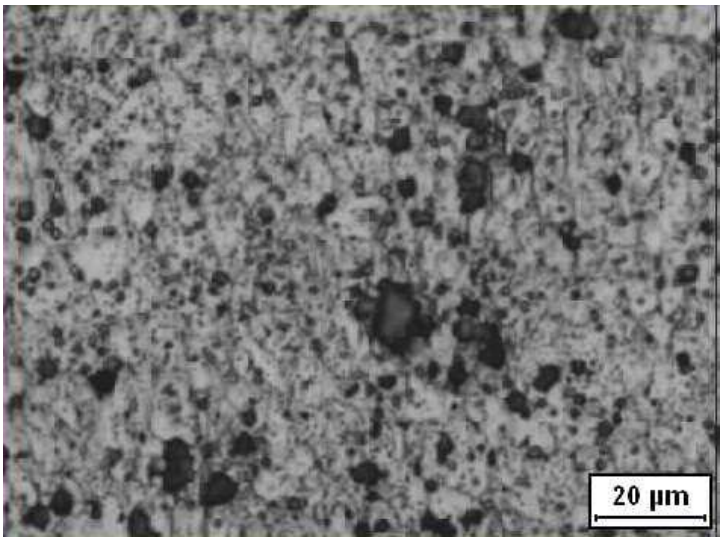

Fig.7	The photomicrograph of pitted Steel-4381 after EN experiment etched electrochemically

JCSE The Journal of Corrosion Science and Engineering
ISSN 1466-8858 Volume 15, Preprint 31 submitted 4 July 2012

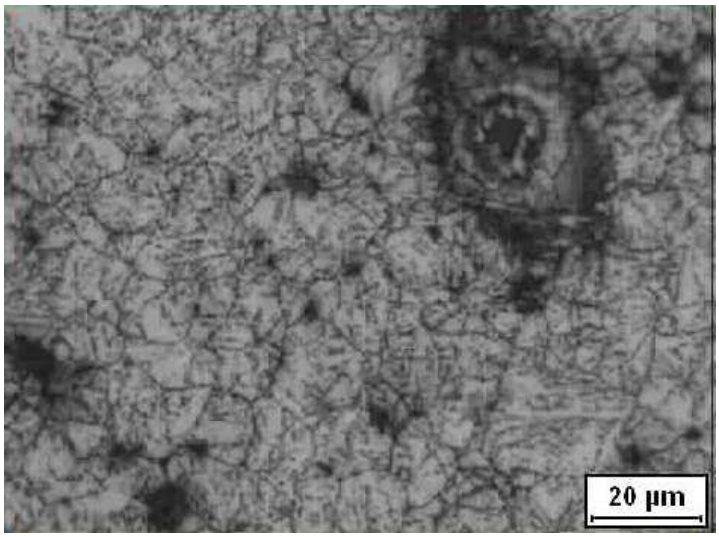

Fig.8	The photomicrograph of pitted Steel-4382 after EN experiment etched electrochemically

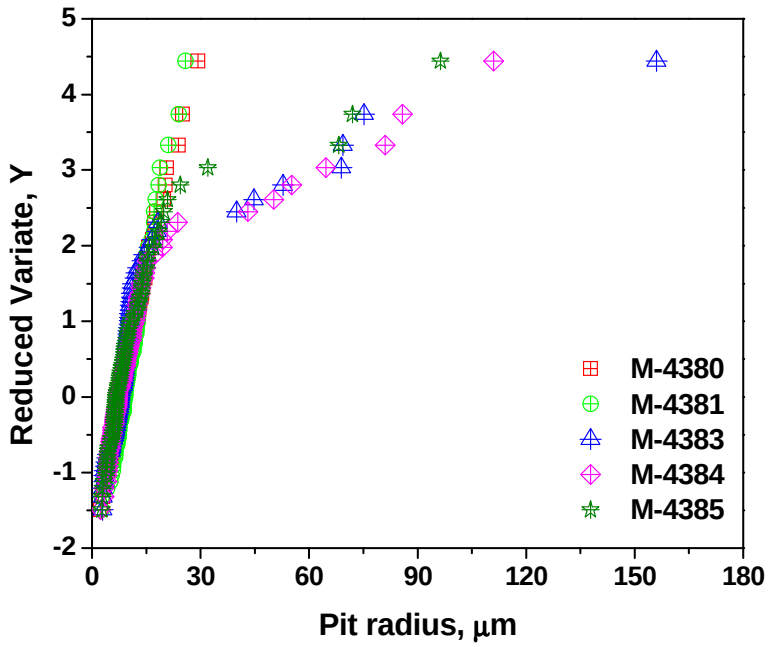

Fig.9	The Gumbel distribution plots showing pit radius vs. reduced variate for steels in 0.05M NaCl solution.

JCSE The Journal of Corrosion Science and Engineering
ISSN 1466-8858 Volume 15, Preprint 31 submitted 4 July 2012

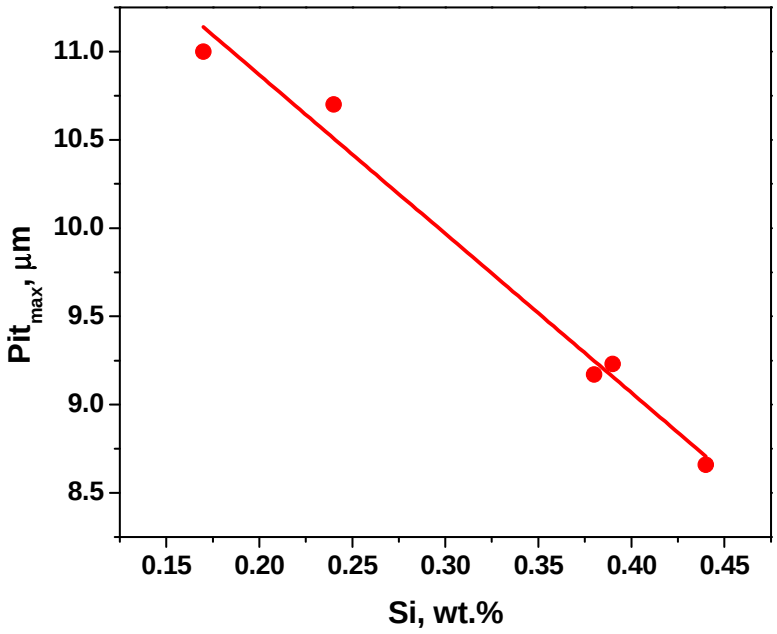

Fig.10	The Pitmax as a function of Si content for the steel in 0.05M NaCl Solution